Solid Earth, 16, 663–680, 2025

Solid Earth Open Access

# What do arc magmatism trace-element patterns and Sr–Nd–Pb isotopic data reflect? Insights from the Urumieh–Dokhtar magmatic arc of Iran

**Mohammad Reza Ghorbani**[1], **Meysam Akbari**[1,2], **Ian T. Graham**[3], **Mathieu Benoit**[4], **and Fatemeh Sepidbar**[5]

[1]Department of Geology, Tarbiat Modares University (TMU), Tehran, 14115-175, Iran
[2]Research Institute for Earth Sciences, Tehran, 13185-1494, Iran
[3]Earth and Sustainability Science Research Centre, School of Biological, Earth and Environmental Sciences, The University of New South Wales, Sydney, NSW 2052, Australia
[4]Géosciences Environnement Toulouse (GET), Observatoire Midi Pyrénées (OSU-OMP), Université de Toulouse, CNRS, IRD, 14 Avenue E. Belin, Toulouse, 31400, France
[5]Department of Geology, Faculty of Sciences, Ferdowsi University of Mashhad, Mashhad, Iran

**Correspondence:** Mohammad Reza Ghorbani

Received: 3 October 2024 – Discussion started: 19 November 2024
Revised: 23 March 2025 – Accepted: 10 April 2025 – Published: 14 July 2025

**Abstract.** Mafic volcanic rocks from the Cenozoic Urumieh–Dokhtar magmatic arc (UDMA) of Iran, a segment of the Alpine–Himalayan orogenic belt, provide rather restricted ranges of trace-element abundances and patterns as well as Sr–Nd–Pb isotopic signatures. However, they are distinct enough to help characterize the geochemical signatures inherited from their arc system components. The volcanic rocks are classified into three series: the LILE-rich, LILE-poor, and incompatible trace-element-rich series (ITE-rich series, which includes samples with OIB-like – oceanic-island basalt – patterns). The LILE-rich series is derived from a mantle source metasomatized by fluid-rich slab partial melts, whereas the LILE-poor series, high in immobile and highly incompatible elements that include La and Ce, is derived from a mantle source metasomatized by fluid-poor slab partial melts. Slab melting is favored by the young, hot slab subduction of a then narrow, contracting Neotethyan oceanic plate. The ITE-rich series bear the signatures of mantle metasomatized by slab partial melts that were induced by, and reacted with, asthenospheric mantle that ascended through a slab window or rupture. Given almost primitive geochemical signatures of the mafic rocks, the Sr–Nd isotopic modeling indicates mantle wedge : slab melt : sediment melt contributions of 45 : 27.5 : 27.5 and 55 : 09 : 36 for the LILE-rich and LILE-poor series respectively. The mafic volcanic rocks, which extend from the mantle array (i.e., the NHRL; Northern Hemisphere reference line) toward an enriched mantle, on the Pb–Pb isotopic plots, further support this finding. Eocene to Early Miocene ages for these three series favor intermittent volcanism of each rock series over an extended period of time, rather than single episodic magmatism for each geochemically distinct magma series. Dominance of LILE-rich series rocks in the northern part of the study area (the Kahak area) points to a more hydrous, more altered slab compared to the slab beneath the central part, where the LILE-poor series is dominant.

## 1 Introduction

The origin and evolution of subduction-related or arc-affinity volcanic rocks have been the subject of scrutiny for many years (Cross and Pilger, 1982; Hildreth and Moorbath, 1988; Benoit et al., 2002; Bouilhol et al., 2013; van Hinsbergen et al., 2020), and those from the Cenozoic Urumieh–Dokhtar magmatic arc (UDMA) of Iran are no exception (Berberian and King, 1981; Agard et al., 2005; Chiu et al., 2013; Ghorbani et al., 2014). However, no major review has been undertaken to present an overview of the compositional spectrum and primitive end-members for the magmatic, mainly

volcanic rocks in the UDMA. Involvement of a number of distinct source components, such as mantle, slab fluids, or partial melts derived from the subducting slab and overlying sediments, leads to a wide variation in chemistry, particularly trace-element abundances and patterns of subduction-related volcanic rocks (Pearce et al., 1990; Ewart et al., 1998; Xia, 2014). Revealing the source components of volcanic rocks is not only one of the most important tasks but also one of the most difficult in the study of magmatic arcs. Moreover, the source components are usually obscured by secondary or differentiation processes. This is especially the case for active continental margins, where the overlying thick crustal rocks may undergo partial melting to further contribute to the magmatism (Spikings et al., 2015; Di Giuseppe et al., 2021). Focusing on the "most mafic" volcanic rocks, represented by the samples in the 48 wt % to 57 wt % silica range, is a reliable approach that avoids secondary processes that blur pristine magmatic components.

Based on the major- and trace-element and Sr–Nd–Pb isotopic data from a collection of mafic volcanic rocks sampled from multiple areas across the central part of the UDMA (Fig. 1), this study tries to infer some key implications as to the nature of the geodynamic evolution as well as mantle and crustal source regions that melted and/or dehydrated to produce them. In order to achieve this goal, (1) abundances and patterns of incompatible trace elements and Sr–Nd–Pb isotopic ratios in the mafic volcanic rocks were investigated and three distinct series were found to occur, and (2) considering the likely involvement of the mantle, slab fluids, slab melts, and crustal components as well as the radiometric ages compiled from recent studies, a petrogenetic model is presented that sheds light on the geodynamic evolution of the three rock series.

## 2 Geology of the study area

As a part of the Alpine–Himalayan Belt, the Zagros Orogeny stretches for nearly 2000 km from northwest to southern Iran. This orogeny is the consequence of subduction of the Neotethyan oceanic plate beneath central Iran and the final collision of the Arabia and Eurasia plates (Berberian and King, 1981; Alavi, 1994; Mohajjel and Fergusson, 2000). The Zagros Orogeny comprises three sections: the Zagros Fold and Thrust Belt (ZFTB), the Sanandaj–Sirjan Zone (SSZ), and the UDMA (Fig. 1a). The UDMA, also known as the central Iran magmatic belt, occurs as a thick mainly Eocene-to-Miocene volcanic succession of up to 3000 m that is intruded by plutonic bodies of mainly Oligocene-to-Miocene age. An active continental-margin model (Berberian and Berberian, 1981; Moinevaziri, 1985) for the subduction predominates, though a few studies report some similarities to island-arc magmatism (Ghorbani, 2006; Shahabpour, 2007).

Based on fossiliferous interbeds, the UDMA volcanic succession has been traditionally attributed to the Eocene (e.g., Berberian and King, 1981; Emami et al., 1993) and is divided into six units, $E_1$–$E_6$, on the geological maps drafted by the Geological Survey of Iran (cf. Fig. S1 in the Supplement for lithostratigraphic columns of different segments of the study area). Verdel et al. (2011), based on the dominantly Eocene ages obtained for the volcanic rocks from the Tafresh area (i.e., the northernmost part of the central UDMA), introduced the Eocene flare-up model as being responsible for the Cenozoic magmatism of the UDMA. In this model, extension induces partial melting of a metasomatized mantle source, producing Eocene calc-alkaline volcanic rocks. This model suggests gradual slab rollback caused asthenospheric upwelling and triggered OIB-affinity volcanic rocks in the Oligocene.

Multiple age-dating of the volcanic rocks from the UDMA prompted Chiu et al. (2013) to infer that magmatic flare-up was not only limited to the Eocene but also extended into the Oligocene. Further age dating by Ghorbani et al. (2014) extended the widespread magmatic activity in the UDMA into the Miocene. Having presented the age-dated samples from the central UDMA on a generalized stratigraphic column that was compiled based on geological maps, Ghorbani et al. (2014) implied there was a discrepancy. The discrepancy in ages (i.e., the difference between the real age and the presumed Eocene age) indicates the necessity for a revision of the $E_1$–$E_6$ divisions. An improvement in the stratigraphic column of the UDMA has recently begun to emerge (see Fig. 2 in Sepidbar et al., 2021): Oligocene–Miocene magmatic records grow at the expense of Eocene magmatic records. Moradi et al. (2021) also reported Miocene ages for volcanic rocks from the Neragh area of the central part of the UDMA. Adakitic rocks have also been reported from the central UDMA (Omrani et al., 2008; Ghorbani and Bezenjani, 2011; Ghorbani et al., 2014; Ahmadian et al., 2016); these, however, postdate the Middle Miocene and have been attributed to high-pressure slab melting.

The present literature on the evaluation of the compositional aspects of the magmatic rocks from the UDMA is limited. Volcanic rocks with negative Nb–Ta anomalies are attributed to subduction (Pearce, 1982; Kelemen et al., 2005), whereas some rocks with higher Nb–Ta abundances have been regarded as being derived from an asthenospheric mantle source (Verdel et al., 2011; Yeganehfar et al., 2013). A few studies on the UDMA include Sr–Nd–Pb isotopic data on the mafic volcanic rocks (Yeganehfar et al., 2013; Jolani Varzeghani, 2017; Khodami, 2019; Sepidbar et al., 2019; Moradi et al., 2021); these works collectively attribute the volcanic rocks to the mixing of varying, marginal proportions of crustal melts with dominantly mantle-derived partial melts in a subduction setting.

The UDMA is mainly dominated by intermediate to felsic volcanic and pyroclastic rocks. These include andesites–trachyandesites; dacites–rhyolites; and tuffs, tuff breccias,

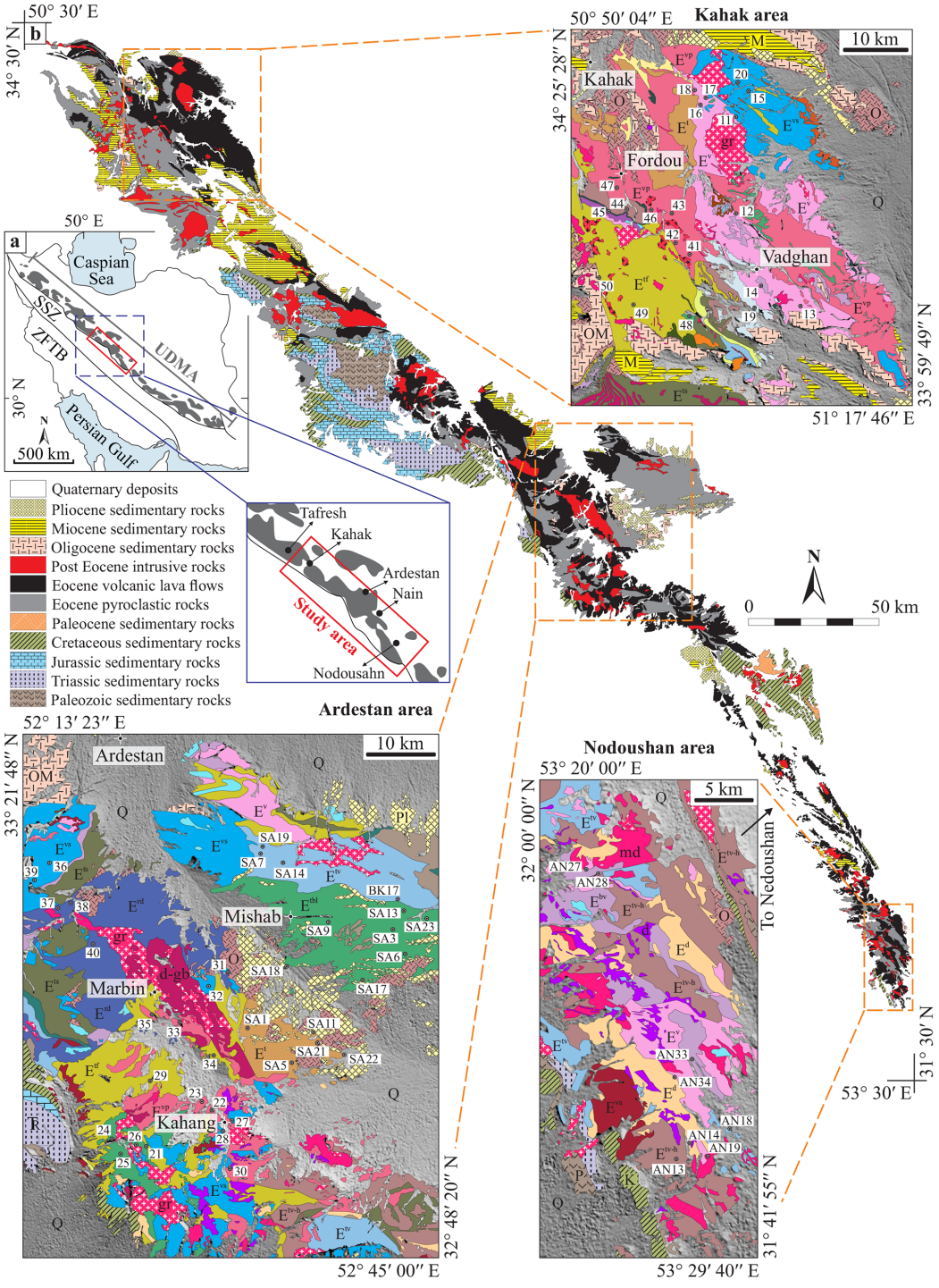


**Figure 1. (a)** Regional tectonomagmatic units of Iran (Alavi, 1994). The gray fields show the Urumieh–Dokhtar magmatic arc (UDMA). Abbreviations: SSZ refers to the Sanandaj–Sirjan Zone and ZFTB refers to the Zagros Fold and Thrust Belt. **(b)** Simplified geological map of the central UDMA based on the geological maps on a scale of 1 : 100 000 for Kahak (Ghalamghash et al., 1988), Kashan (Radfar and Alaie-Mahabadi, 1993), Natanz (Khalatbari Jafari and Alaie-Mahabadi, 1995), Tarq (Zahedi and Rahmati, 2002), Ardestan (Radfar and Amini Chehragh, 1999), Shahrab (Bahroudi and Fonoudi, 1997), Kuhpayeh (Radfar et al., 2002), Kajan (Amini and Amini Chehragh, 2003), Nain (Alaie-Mahabadi and Foudazi, 2004), Sarve-Bala (Amidi et al., 1989), and Kafeh-Taghestan (Ghalamghash et al., 2005). More detailed geological maps are provided for three segments of the central UDMA. Locations of the samples selected for geochemical analyses are also shown. For the legend and the lithostratigraphic columns of these three segments of the central UDMA, see Fig. S1.

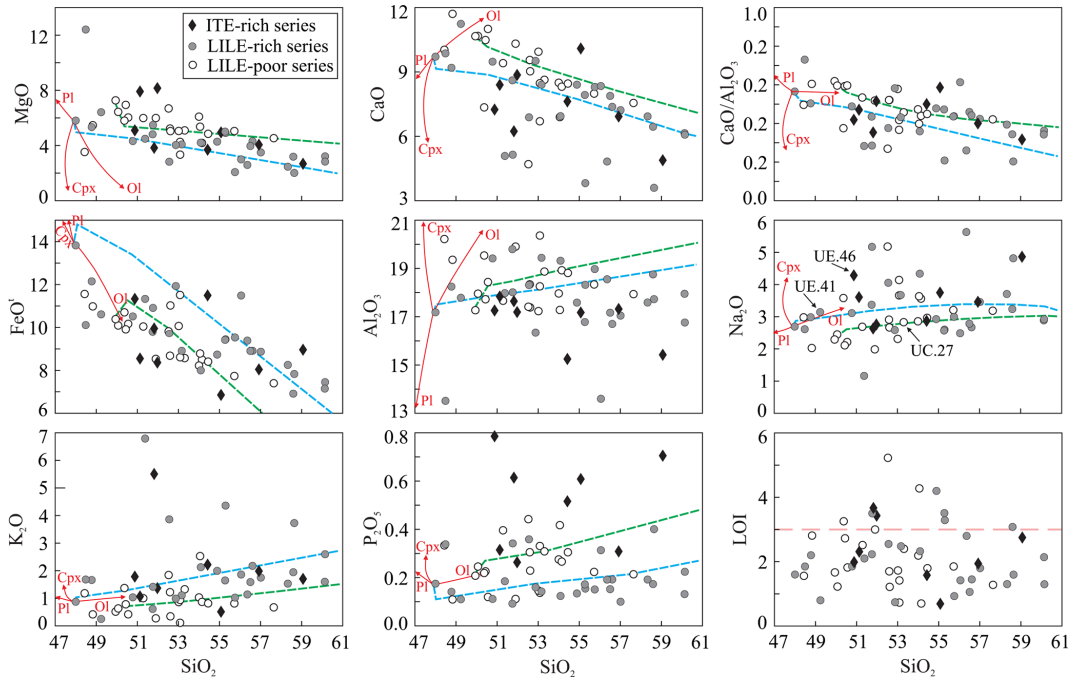


**Figure 2.** Major-element oxides vs. $SiO_2$ variation diagrams for the LILE-poor, LILE-rich, and ITE-rich series from the UDMA. For more details regarding the variation diagrams see Fig. S3a–c. The solid red lines with arrows indicate the effect of 20 % fractional crystallization (FC) of olivine (Ol), clinopyroxene (Cpx), and plagioclase (Pl) on the whole-rock compositions (calculated using MagPath spreadsheet software; Mayborn and Lesher, 2011). The dashed blue line is the calculated liquid line of descent resulting from 83 % fractional crystallization of 0.18 olivine + 0.41 clinopyroxene + 0.40 plagioclase + 0.01 apatite followed by 17 % fractional crystallization of 0.05 olivine + 0.31 clinopyroxene + 0.48 plagioclase + 0.16 Ti–magnetite. The dashed green line denotes the calculated liquid line of descent resulting from 75 % fractional crystallization of 0.25 olivine + 0.41 clinopyroxene + 0.33 plagioclase + 0.01 Ti–magnetite followed by 25 % fractional crystallization of 0.06 olivine + 0.32 clinopyroxene + 0.46 plagioclase + 0.16 Ti–magnetite. The dashed blue and green lines and the calculated liquid lines of descent match well with the trends defined by natural samples from the LILE-rich and LILE-poor series respectively. These FC models imply that the LILE-poor and LILE-rich series were derived from different parental magmas.

and ignimbrites. Mafic volcanic rocks occur sporadically and include basalts, alkali basalts, and trachybasalts. The apparent scarcity of mafic rocks in the UDMA volcanic successions has been a major obstacle in the evaluation of end-members of the source regions and materials that evolved to generate the volcanic successions. The paucity of mafic rocks makes it difficult to follow the melt compositional evolution or liquid line of descent (Wilson, 1989). To overcome this paucity of mafic rocks, the current study carried out widespread sampling from multiple areas across the central part of the UDMA (Fig. 1). This furnished a representative set of the mafic–intermediate volcanic rocks for detailed petrological and geochemical investigations.

The volcanic rocks sampled in this study are lavas ranging in thickness from meters to tens of meters. Porphyritic to aphyric textures of the volcanic rocks confirm their eruptive nature. A simplified geological map of the UDMA is shown in Fig. 1, which is compiled based on the present geological maps (see caption in Fig. 1 for details). The present study area comprises three segments from northwest to southeast; these are Kahak (including Fordou and Vadghan), Ardestan (including Mishab, Marbin, and Kahang), and Nodoushan, respectively (Fig. 1b). Integrating these volcanic segments into a larger tectonic context will be a worthwhile endeavor as a roadmap for future studies.

## 3 Petrographic analysis

Petrography focused on samples of the volcanic series considered representative of the present study areas from the UDMA (Fig. 1b). The basaltic rocks of the present study mostly contain sparse clinopyroxene along with minor plagioclase phenocrysts in a fine-grained groundmass. The mafic–intermediate volcanic rocks are slightly to moderately porphyritic in texture (Fig. S2 in the Supplement). While the groundmass in some samples is almost aphyric, other samples show a cryptocrystalline to microcrystalline groundmass composed of glass, plagioclase, clinopyroxene, and Fe–Ti oxides.

Textural and mineralogical characteristics of the mafic volcanic rocks from the study area are briefly presented in Table 1. Although glass constitutes the major component of

the groundmass, most samples include variable quantities of fine-grained feldspars, clinopyroxenes, and Fe–Ti oxides. Olivine and orthopyroxene phenocrysts are rare, mostly altered, and found as pseudomorphed grains (i.e., replaced by chlorite and other secondary minerals). Glomeroporphyritic textures are found in a few samples and mainly include clinopyroxene and plagioclase. Amphibole was only found in two samples from the Nodoushan area where mafic volcanic rocks are rare and limited to andesitic rocks (see below). Only fresh samples were selected, so secondary minerals such as sericite, chlorite, calcite, and epidote, which are the alteration products of silicate minerals, are rare if present at all. However, before using the geochemical data, the possibility of alteration and its effect on element mobility are discussed below (see Sect. 6.1).

## 4 Methods

A representative set of 66 mafic–intermediate volcanic rocks from the study area was analyzed for major and trace elements (Table S2 in the Supplement). After a detailed examination of the major- and trace-element geochemistry of the rocks, 14 samples were selected for Sr–Nd–Pb isotopic analyses (Table S3 in the Supplement). In order to avoid altered samples, the representative set was selected based on detailed petrographic examinations of 250 thin sections across the region.

### 4.1 Major- and trace-element analysis

Whole-rock analyses for major elements were obtained by x-ray fluorescence (XRF) at the Mark Wainright Analytical Centre, University of New South Wales, Sydney, Australia, following the procedures of Norrish and Hutton (1969). The analyses were carried out on a Phillips PW2400 XRF spectrometer using 40 mm glass disks. Inductively coupled plasma–mass spectrometry (ICP–MS) was used for rare earth and trace-element analyses of the whole-rock samples at the Genalysis Laboratory, Perth, Australia, using the Perkin–Elmer ICP–MS 9000 (i.e., 51 samples marked by numbers in normal fonts in Table S2), and the School of Geography, Earth and Atmospheric Sciences, University of Melbourne, Victoria, Australia, using the NexION 2000 (i.e., for 15 samples marked by numbers in italic fonts in Table S2).

Some accessory minerals are trace-element repositories that resist the mixed acid digest method. To ensure complete digestion while maintaining good sensitivity, a combination digestion method (i.e., a mixed acid digest and multi-fusion) was used. The details are as follows. The pulp was digested in $HNO_3/HClO_4$ on a hot plate and then cooled. HF was added and digestion continued on the hotplate; the mixture was then cooled and salts were leached with an $HCl/HNO_3$ mix on the hotplate. The solution was then cooled and filtered to recover undigested material fused with a minimal Li metaborate–tetraborate flux. The melt was produced and then leached with HCl. Leach solutions were combined for the ICP–MS analysis.

Both in-house and internationally certified standards were analyzed (Table S4 in the Supplement) and gave overall relative procedural errors of better than 3 %. Analytical reproducibility was also examined. For the rare earth and trace elements, errors were evaluated to be better than 3 % except for Nb, Ta, and U (8 %). Duplicate analyses indicate that the errors for major elements are better than 1 % except for alkaline elements (5 %). The whole-rock analysis totals are in the range from 98.79 wt % to 101.83 wt % with a mean of 100.80 wt % (Table S2). The diagrams depicted are based on the major-element analyses recalculated to 100 wt %, on an anhydrous basis.

### 4.2 Sr–Nd–Pb isotopic analysis

The isotopic data were obtained from GET–OMP, Toulouse University (France), using the Thermo Scientific TRITON+ solid source mass spectrometer, following the procedures outlined in Li et al. (2011, 2012). Before measurement, about 100 mg of whole-rock powder was weighed in a Teflon beaker and dissolved in a 1 : 1 mixture of $HF/HNO_3$. After dissolution, samples were diluted in 1 mL 2 % $HNO_3$, and Nd/Sr was extracted from the matrix (2 N $HNO_3$) using a combination of Sr-Spec and TRU-Spec Eichrom resins. Mixed Sr and REE fractions were loaded onto a Re filament and run sequentially (first Sr, then Nd) using a double-Re-filament protocol. Monitoring of the interferences of $^{87}Rb$ and $^{144}Sm$ took place according to the protocol of Li et al. (2012), and the quality and reproducibility of the measurements were controlled using a sequential measurement of isotopic standards (SRM 987 and JNdi), doped isotopic standards (NBS 987 + Rb and JNdi + Sm), and laboratory-dedicated Sr + REE artificial solutions. Standard reproducibilities are $^{87}Sr/^{86}Sr = 0.710280 \pm 15$ for SRM-987 and $0.512100 \pm 10$ for JNdi (pure and doped) and fall within the recommended values. Measured blanks are 25 pg for Nd and 325 pg for Sr. $^{87}Sr/^{86}Sr$ and $^{143}Nd/^{144}Nd$ ratios were normalized to $^{86}Sr/^{88}Sr = 0.1194$ and $^{146}Nd/^{144}Nd = 0.7219$ respectively, after corrections from isobaric interferences using $^{87}Rb/^{85}Sr = 0.387041$ on $^{87}Sr$ and $^{147}Sm/^{149}Sm = 1.08583$ together with $^{147}Sm/^{144}Sm = 4.87090$ for $^{144}Nd$.

Pb fractions have been extracted from the matrix during the same elution protocol as Sr and Nd following the procedure of Pin and Gannoun (2017). Pb isotopes were determined on a Thermo Scientific TRITON+ solid source mass spectrometer using the Rex–Taylor double-spike method. NBS 981 reproducibility for lead ratios is around 100 ppm. Blanks are typically lower than 20 pg.

**Table 1.** Modal mineralogy of LILE-rich, LILE-poor, and ITE-rich series. Petrographic features of the individual samples are provided in Table S1 in the Supplement. Photomicrographs of samples with bold numbers are provided in Fig. S2. The abbreviations Fld, Pl, Cpx, Opx, Ol, Amp, and Opq stand for feldspar, plagioclase, clinopyroxene, orthopyroxene, olivine, amphibole, and opaque minerals respectively.

| Rock series | Sample no. | Texture | Groundmass | Phenocrysts (vol %) |
|---|---|---|---|---|
| LILE-poor | **UC30**, UD32, UD37 | Vitrophyric | Glass ± Fld ± Cpx ± Opq | ≤ 5, Ol ± Pl ± Cpx |
| | UC22, UC25, UC26 **UC27**, **UC28**, UD33, UD36, UD38, SA1, SA9 | Porphyritic | Cryptocrystalline to microcrystalline Glass + Fld + Opq ± Cpx | ≤ 5, Pl ± Ol ± Opx ± Cpx ± Opx |
| | UC23, UC24, UD34, **UD35**, UD39 | Porphyritic | Cryptocrystalline to microcrystalline Glass + Fld + Cpx + Opx | < 10, Pl ± Cpx ± Ol ± Opx ± Opq |
| | UC21, UD31 | Porphyritic | Cryptocrystalline Glass + Fld ± Cpx ± Opx | < 20, Pl ± Ol ± Cpx |
| | SA13, SA23 | Microgranular Fld + Opq ± Ol ± Opx | ± Glass | |
| LILE-rich | AN14, AN18, AN33 UE41 | Vitrophyric | Glass ± Fld ± Opq | ≤ 5, Pl ± Cpx ± Opx ± Opq |
| | UB13, UB14, UE42 | Porphyritic | Microcrystalline to cryptocrystalline Fld ± glass ± Cpx ± Opx | ≤ 5, Pl ± Cpx |
| | UB12, UB15, **UB16**, **UB18**, UB19, UB20, SA7, **SA18**, AN34, UE45, UE47, **UE48**, UE50 | Porphyritic | Cryptocrystalline Glass + Fld ± Cpx ± Opx | < 15, Pl ± Cpx ± Ol ± Opx ± Amp |
| | UB17, SA19, UE44 | Porphyritic | Glass + Fld ± Cpx ± Opq | < 25, Pl ± Opx ± Opq |
| | AN13 | Porphyritic | Glass | < 10, Pl + Amp + Cpx + Opx |
| | AN27 | Microgranular Pl + Cpx + Amp + Opq | | |
| | UE43, UE49 | Microgranular (Pl + Cpx + Opx) | | |
| ITE-rich | **SA14**, SA17 | Vitrophyric | Cryptocrystalline Glass ± Fld ± Opq | ≤ 5, Pl |
| | UE46, **SA21** | Porphyritic | Cryptocrystalline to microcrystalline Glass + Fld ± Cpx + Opq | ≤ 5, ± Pl ± Ol |
| | UB11, SA3, **SA11** | Porphyritic | Cryptocrystalline Glass + Fld ± Cpx ± Opq | < 15, Pl ± Cpx ± Ol ± Opx ± Opq |
| | **SA6** | Microgranular Fld + Opq | | |

## 5 Results

### 5.1 Major and trace elements

The mafic volcanic rock totals vary in the 98.28 wt % to 101.82 wt % range with an average of 100.46 wt %. Most samples contain less than 3 wt % LOI (loss on ignition), an indication of the reliability of their geochemistry (i.e., the rocks have maintained their original geochemical characteristics; see the subsection Alteration in the Discussion section). In Harker variation diagrams, CaO, MgO, and $FeO^t$ show broadly decreasing trends with increasing $SiO_2$, whereas $Na_2O$ and $K_2O$ show increasing trends (Fig. 2). These covariations are well defined for specific areas (cf. Figs. 2 and S3a, b in the Supplement). Volcanic rocks from Marbin and Kahang show higher Mg and Ca and lower Fe, Na, and K compared to the Fordou and Vadghan areas (cf. Fig. S3a and b). These largely correspond to the volcanic rocks from the LILE-poor and LILE-rich series (see below) respectively.

The mafic volcanic rocks from the study area can be divided into three distinct compositional series based on their primitive mantle-normalized trace-element patterns (Sun and McDonough, 1989). In Fig. 3, these are termed the LILE-poor, the LILE-rich, and the ITE-rich series (LILE and ITE refer to large-ion lithophile elements and incompatible trace elements respectively). The LILE-poor and LILE-rich series show negative Nb–Ta anomalies, which clearly favor an arc setting. These rocks belong to the subalkaline series and further show calc-alkaline affinities. The LILE-poor series is rather depleted in Rb, K, and HREE compared to the LILE-rich series. The ITE-rich series is enriched in the lithophiles, La, Ce, Pb, Sr, and P with both calc-alkaline and alkaline features. Mafic volcanic rocks from the ITE-rich series are sometimes enriched in Nb–Ta (Fig. 3; diagrams in the upper row).

Volcanic rocks exhibiting these three patterns (i.e., the LILE-poor, LILE-rich, and ITE-rich series) also show some major-element geochemical distinctions. Rocks from the LILE-poor series show higher Mg and Ca and lower Fe and alkaline elements compared to the LILE-rich series samples (Figs. 2 and S3a–c). Details of the mafic rock variation diagrams for three segments of the study area are shown in Fig. S3a–c; these are Kahak (Fodou and Vadghan), Ardestan (Mishab, Marbin, and Kahang), and Nodoushan (Fig. 1). Importantly, the mafic volcanic rocks of the three series/patterns occur across all segments of the study area, though they vary in their different proportions.

### 5.2 Sr–Nd–Pb isotopic data

Sr–Nd–Pb isotopic ratios were determined for a set of 14 mafic volcanic rocks (Table S3) from the study areas belonging to the LILE-rich series (four samples), the LILE-poor series (six samples), and the ITE-rich series (four samples). The ranges of measured Sr isotopic ratios for the LILE-rich, the LILE-poor, and the ITE-rich series are 0.70562 to 0.706085, 0.705099 to 0.706263, and 0.704443 to 0.705561 respectively. The ranges of measured Nd isotopic ratios for the LILE-rich, the LILE-poor, and the ITE-rich series are 0.512715 to 0.512786, 0.512607 to 0.512766, and 0.512673 to 0.512804 respectively.

Only four out of the fourteen samples are age-dated using the whole-rock K–Ar method (Ghorbani et al., 2014). These range from 18.2 to 34.6 Ma, similar to the ages obtained for the UDMA mafic volcanic rocks by Yeganehfar et al. (2013). None of the three series of volcanic rocks (the LILE-rich series, the LILE-poor series, or the ITE-rich series) appear to be confined to a particular time span. Mafic volcanic rocks of the same compositional affinities from the central UDMA studied by Moradi et al. (2021) further extended this age range from 21.5 to 60.0 Ma. Therefore, an average age of 35 Ma is suggested for calculation of the initial Sr, Nd, and Pb isotopic ratios. The ranges of initial Sr isotopic ratios for the LILE-rich, the LILE-poor, and the ITE-rich series are 0.705448 to 0.706017, 0.705044 to 0.706237, and 0.704379 to 0.705505 respectively. The ranges of initial Nd isotopic ratios for the LILE-rich, the LILE-poor, and the ITE-rich series are 0.512677 to 0.512746, 0.512573 to 0.512729, and 0.512637 to 0.512772 respectively (Table S3).

The mafic volcanic rocks from the study area plot on the same area of the Sr–Nd isotopic plot as other orogenic volcanic rocks and on the same area as other mafic volcanic rocks from the UDMA (Fig. 4). Toward lower Sr isotopic ratios, data points from the three series converge to share a narrow space in the mantle array close to the Bulk Silicate Earth (BSE). The Sr–Nd isotopic variation trends expand toward higher Sr and lower Nd isotopic ratios (Fig. 4a). These volcanic rocks display moderately radiogenic Pb compositions ($^{206}Pb/^{204}Pb_{(i)} = 18.52–18.72$, $^{207}Pb/^{204}Pb_{(i)} = 15.51–15.69$, and $^{208}Pb/^{204}Pb_{(i)} = 38.33–38.80$; Table S3). On Pb–Pb isotopic plots, the mafic volcanic rocks form linear trends stretching from the mantle array (i.e., the NHRL; Northern Hemisphere reference line) toward enriched mantle above the reference line (Fig. 4b and c).

## 6 Discussion

### 6.1 Alteration

The development of secondary minerals in the mafic volcanic rocks from the study areas is strictly limited to a few pseudomorphs of primitive olivine and orthopyroxene (see Sect. 3, "Petrographic analysis"). This along with LOI values lower than 3 wt % in most of the samples (i.e., in 55 out of 66 samples) indicates negligible alteration effects. In addition, most of the samples from the LILE-poor series have the same LOI abundances as the samples from the LILE-rich series (Figs. 2 and S3a, b). These overlapping volatile contents do not sup-

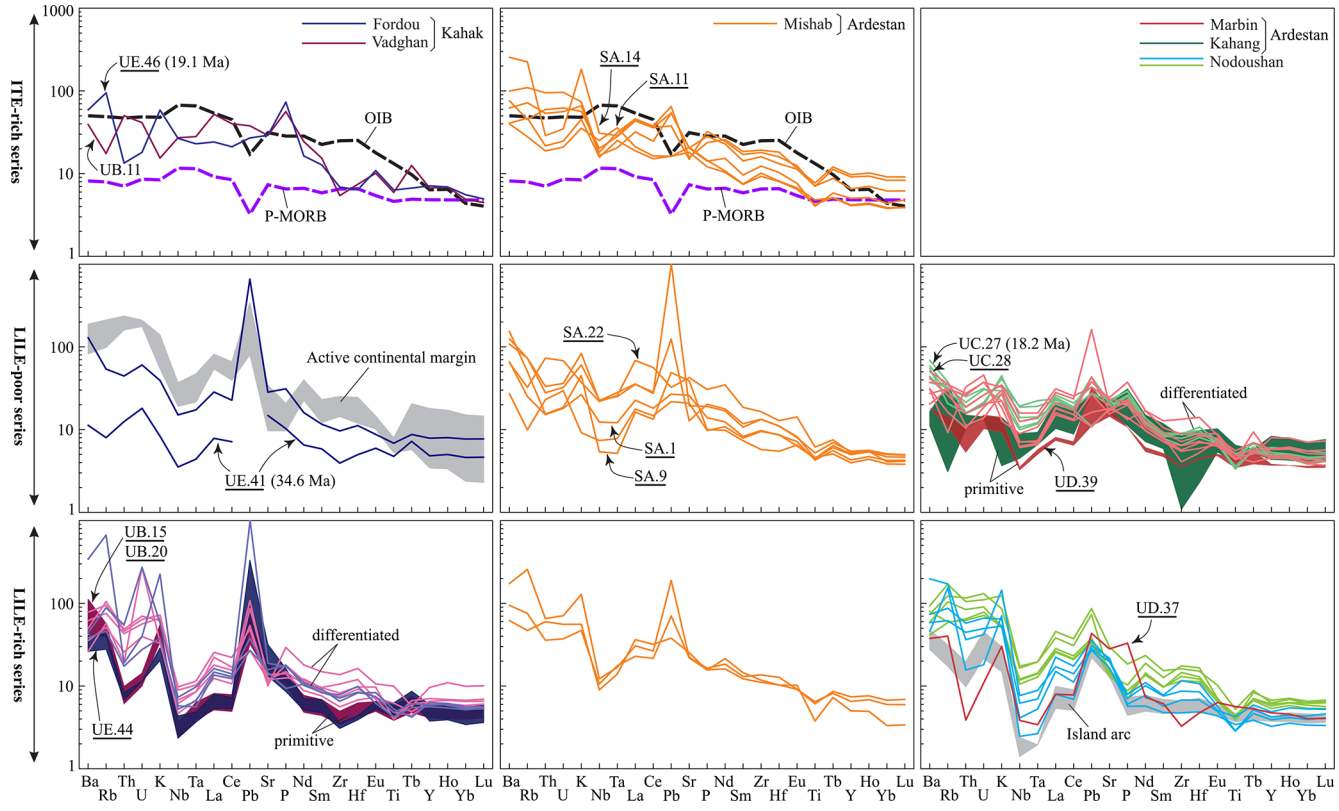


**Figure 3.** Primitive-mantle-normalized trace-element patterns for the Kahak (including Fordou and Vadghan), Ardestan (including Mishab, Marbin, and Kahang), and Nodoushan mafic volcanic rocks. These are classified into the LILE-rich, LILE-poor, and ITE-rich series. Differentiated samples are shown in pale colors as compared to the more primitive samples, which are shown in dark colors. Underlined sample numbers indicate the mafic volcanic rocks for which Sr–Nd–Pb isotopic data were obtained in the current study (see Table S3 and Fig. 4). Age-dated samples are from Ghorbani et al. (2014). For other age-dated samples from the study areas see Figs. S4 and S5. Normalization values for the primitive mantle (PM) and trace-element abundances for OIBs and P-MORBs (plume-type mid-ocean ridge basalt) (diagrams in the upper row) are from Sun and McDonough (1989). Trace-element abundances for the island-arc basalts (lower-right diagram) and active continental-margin basalts (left-side diagram in the second row) are from Jicha and Singer (2006) and Straub et al. (2015) respectively.

port a correlation between the LOI and alkali contents (see Fig. 2), a correlation usually regarded as a measure of the extent of alteration (e.g., Dong et al., 2017). In Mishab, the LILE-poor series samples have the highest LOI (Fig. S3a); this does not support a correlation between alkali content and LOI and provides yet additional evidence as to the lack of significant alteration effects.

### 6.2 Primitive signatures

Mafic magmatic rocks are not common in magmatic arcs (e.g., Plank and Langmuir, 1988). Subduction- or arc-related volcanic successions are dominated by intermediate to felsic volcanic products, which are conventionally viewed as derivatives of arc basaltic magmas triggered by partial melting of metasomatic components in the mantle wedge (Gill, 1981; Plank and Langmuir, 1988; Benoit et al., 2002; Streck et al., 2007). A thick continental lithosphere and/or crust promotes the development of high-level magma chambers that prohibit rapid magma ascent and lead to significant magmatic differentiation – namely assimilation–fractional crystallization (AFC) – and thus mask most of the original mantle source signatures (Plank and Langmuir, 1988; Farner and Lee, 2017). MgO contents of the volcanic rocks from the study area are rather low (< 7 wt %), indicating that even the most mafic samples experienced some degrees of differentiation. It is however noted that some of the least differentiated samples from magmatic arcs maintain the trace-element signatures of primitive melts. As measures of the rather primitive nature of the volcanic rocks, their Mg numbers are presented in Table S2. Non-cumulative, rather aphyric or slightly porphyritic UDMA mafic rocks with low LOI contents and minor or no alteration are examined here to infer implications as to the geochemical signatures of their primitive melts.

It is noted above that the mafic volcanic rocks from the study area are representative of three distinct trace-element patterns, namely the LILE-poor, LILE-rich, and ITE-rich series. Samples from the LILE-poor and LILE-

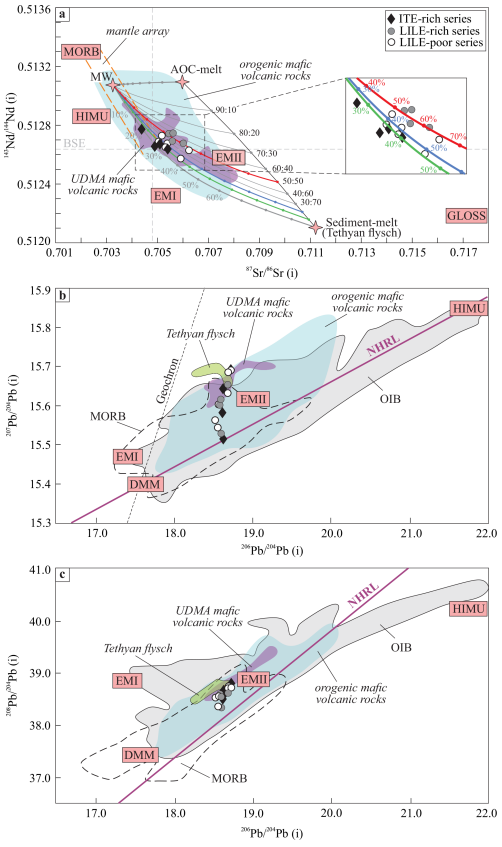


**Figure 4.** **(a)** Initial Sr–Nd isotopic-ratio plot for the mafic volcanic rocks from the study areas, showing a three-component mixing model, determined using a simple mass-balance approach (Powell, 1984), for the LILE-rich, LILE-poor, and ITE-rich series of mafic volcanic rocks from the central UDMA. See Table S5 in the Supplement for further details on modeling parameters. **(b)** Plots of $^{207}Pb/^{204}Pb$ vs. $^{206}Pb/^{204}Pb$ and **(c)** $^{208}Pb/^{204}Pb$ vs. $^{206}Pb/^{204}Pb$ ratios for the mafic volcanic rocks from the study areas. Average values for DMM (depleted MORB mantle), HIMU (high $\mu$; $\mu = {}^{238}U/^{204}Pb$), EMI (enriched mantle 1), and EMII (enriched mantle 2) are calculated based on the samples presented in Akbari et al. (2023), which include a comprehensive database of a variety of basalts. GLOSS (global subducted sediment) values are adapted from Plank and Langmuir (1988). The fields for OIBs (oceanic-island basalts) and MORBs (mid-ocean-ridge basalts) are from Stracke et al. (2003, 2005), Chauvel et al. (2008), and references therein. The NHRL (Northern Hemisphere reference line) is adapted from Hart (1984). The mantle wedge data are represented by the averages of the Kamchatka arc volcanic rocks (Kepezhinskas et al., 1997), the altered oceanic crust (AOC) data are adapted from Hauff et al. (2003), and the Tethyan flysch sandstone sample (06FL03) from Serbia is adapted from Prelević et al. (2008). For comparison of the data achieved in the present study with the published isotopic data for the western Nain (Yeganehfar et al., 2013) and Nodoushan (Jolani Varzeghani, 2017) areas, see Fig. S6. The field for orogenic mafic volcanic rocks is adapted from the GEOROC database. The distribution of nearly coeval mafic volcanic rocks from UDMA (Omrani et al., 2008; Yeganehfar et al., 2013; Shafaii-Moghadam et al., 2014; Jolani Varzeghani, 2017; Khodami, 2019; Rabiee et al., 2020; Moradi et al., 2021) is also shown for comparison. See text for more details.

rich series are marked by a distinctive negative Nb–Ta anomaly, characteristic of subduction-related settings (Fig. 3; see lower-right and middle left diagrams for island-arc and active continental-margin volcanic rock trace-element patterns respectively). The LILE-poor series are depleted in the lithophiles, whereas the LILE-rich series are enriched in the lithophiles. The trace-element pattern for the ITE-rich series is significantly different; it is enriched in the lithophiles, La, Ce, Pb, Sr, and P. Samples from the ITE-rich series are rather enriched in Nb–Ta and present OIB-like trace-element patterns (Fig. 3; diagrams in the upper row).

The LILE-poor and LILE-rich series trace-element patterns span a wide spectrum from an overall low trace-element abundance to an overall high/elevated trace-element abundance. The patterns with an overall low trace-element abundance (i.e., of $< 10$ times that of the primitive mantle) show less differentiated signatures (e.g., slight or no negative Sr and Ti anomalies) and are suggested to represent more primitive partial melts. The low trace-element abundance patterns are likely to imply high-degree partial melts (Wilson, 1989). Higher-degree partial melts show lower trace-element abundances as well as evidence supporting the exhaustion of fusible mantle mineral phases (Ghorbani and Middlemost, 2000). A pronounced negative anomaly in Zr–Hf in some of the UDMA mafic volcanic rocks with an overall low trace-element abundance pattern (Fig. 3) appears to indicate the significant contribution of a mineral phase that bears a negative Zr–Hf anomaly. The gradual consumption and final disappearance of clinopyroxene in the mantle source, as the major participating phase, could impose such a low Zr–Hf signature (Linnen and Keppler, 2002; Atanasova et al., 2020) on the partial melt produced. Alternatively, it may indicate metasomatism by slab partial melts in the source mantle of the LILE-poor series. Metasomatism by slab partial melts is associated with the development of Al-rich orthopyroxene and Mg-rich amphibole in the mantle (Schiano et al., 1995; Kepezhinskas et al., 1995; Szabó et al., 2004). This contracts the clinopyroxene (Cpx) stability field so that the LILE-poor series parental melts portray signatures of Cpx exhaustion.

Most of the mafic volcanic rocks from the study area show large negative anomalies for Th but mild or no anomaly for U, similar to island-arc volcanics (Hawkesworth et al., 1997). This is because Th behaves like HFSEs (high field strength element), whereas U is mobilized by fluids. However, a few samples from the LILE-poor series show positive Th–U anomalies (Fig. 3). One of these samples shows the highest LREE and P abundances amongst the mafic volcanic rocks (sample SA.22; Fig. 3). These may indicate apatite involvement in the petrogenesis of the mafic volcanic rocks with positive Th–U anomalies. Apatite shows extremely high partition coefficients for Th, U, and LREE (O'Reilly et al., 1991). Morishita et al. (2003) found that apatite development in the Finero peridotite is due to a metasomatizing agent derived from subducting "slab possibly containing small quantity of sediment", a condition supported by the isotopic mod-

eling of source end-members for the mafic volcanic rocks from the study area (see Sect. 6.6).

### 6.3 Does fractional crystallization provide an interseries link?

The fact that two series of the samples with the most primitive geochemical signatures (i.e., from the LILE-poor and LILE-rich series) show significant differences in LILE implies the differences/distinctions are inherited from the source. In other words, more primitive samples from these two series best represent their compositional distinctions. Hence, the LILE-poor and LILE-rich series are likely rooted in different source regions. One might challenge this hypothesis and assign the geochemical differences between the two series to differentiation from a single parental melt. Fractionation of the liquidus phases crystallizing from primary mafic melts (i.e., Ol, Opx, Cpx, and Pl; a single phase or a mineral assemblage) may explain some geochemical differences between the two series. Fractionation of $\mathrm{Ol} + \mathrm{Pl} \pm \mathrm{Cpx}$ from an assumed primary mafic melt can explain the major-element geochemical evolution from the LILE-poor series to the LILE-rich series rocks (i.e., decreasing melt Mg and Ca and increasing Fe and alkaline elements). However, this model is not able to explain the distinction/differences between the trace-element abundances and patterns of the two series. Such a differentiation model is expected to produce a series of parallel trace-element patterns, wherein the abundances of nearly all incompatible trace-elements (i.e., with the exception of P and Sr due to the fractionation of apatite and plagioclase respectively) increase as differentiation proceeds. Moreover, the differentiation model is not able to explain some other issues as follows: (1) negative Th anomalies of the LILE-rich series samples are not consistent with their more differentiated nature. Th is a highly incompatible element and is expected to increase with differentiation. Although Th can be compatible in apatite, the rather constant and minimal $P_2O_5$ abundances in the LILE-rich series do not support apatite fractionation. (2) The volcanic rocks representing the LILE-poor and LILE-rich series stretch parallel to each other across the compositional spectrum at the same silica range (Fig. 2). This is more consistent with the concurrent evolution of both series rather than one being the differentiation product of the other.

As noted above, the LILE-poor and LILE-rich interseries geochemical differences are unlikely to have been interconnected (i.e., the latter is not developed by differentiation of the former). Rather, the two series bear some primitive signatures and are likely derived from two distinct source-mantle regions. Nevertheless, the LILE-poor and LILE-rich intraseries geochemical variations appear to have been developed by differentiation through fractional crystallization (FC). The intraseries FC model is supported by the following five observations: (1) the presence of Ol, Opx, Cpx, Pl, and Fe–Ti oxide phenocrysts in the UDMA volcanic rocks. (2) The development of elevated, parallel trace-element patterns in the more evolved samples of the respective series (i.e., the LILE-poor and LILE-rich series; Fig. 3). (3) The gradual decrease in some trace elements which have high Kd for the fractionated minerals (e.g., development of negative Ti anomalies) in the more evolved samples. (4) The plots of differentiation indices versus the Sr and Nd isotopic ratios confirm the dominance of FC with little or no crustal contamination in the evolution of the volcanic rock series from the study area (Fig. 5; for details on the one sample from the ITE-rich series and the two samples from the LILE-poor series, which are marked with arrows and show different geochemistry as compared to the mainstream series, see Sect. 6.5 and the caption under Fig. 5 respectively). (5) Fractional crystallization modeling using the MagPath algorithm (Mayborn and Lesher, 2011) demonstrates different liquid lines of descent for the LILE-rich and LILE-poor series, developed as a result of differentiation of distinct mineral assemblages (see Fig. 2 caption for details). Pb isotopic ratios as more sensitive tools for the detection of crustal components, however, indicate some crustal contamination. For most samples, decreasing $^{207}Pb/^{204}Pb$ with increasing silica (Fig. 5) indicates interaction with un-radiogenic lower crust.

Mafic volcanic rocks with the most primitive geochemical signatures are presented in the current study. Further assurance as to the primitive nature of the ternary classification of the volcanic rocks from the study area (i.e., that the geochemical distinction between these three rocks series is not the artifact of fractional crystallization) is provided by a series of plots where mafic samples define distinct groupings/series. $SiO_2$ versus Ba/Nb or Ba/La helps distinguish the LILE-rich from the LILE-poor series (Fig. 6a and b), whereas $SiO_2$ versus Nb or Zr helps distinguish the ITE-rich series from the other two series (Fig. 6c and d). However, Nodoushan volcanic rocks contain $> 54\,\%$ silica and are rather differentiated. This is indicated by the Nodoushan rocks having pronounced negative anomalies for Ti and P as well as their elevated trace-element patterns (Fig. 3). In fact, Nodoushan rocks constitute two sets of compositional variations; samples with larger negative Sr anomalies (i.e., the more differentiated set) are richer in incompatible trace elements compared to the more primitive set. In Fig. 3 these are shown by green and blue patterns respectively. The more differentiated set shows lower Al abundances attesting to the higher degree of plagioclase differentiation (Fig. S3b).

### 6.4 Mantle metasomatism by fluid-rich slab melt and fluid-poor slab melt furnishing sources of the LILE-rich and LILE-poor series respectively

Different modes of trace-element enrichment (i.e., by fluids/melts released from the subducting slab) in the source mantle may be responsible for the development of the LILE-poor and LILE-rich series melts. Melting of the mantle metasomatized by fluid-rich slab melt is suggested to have produced the

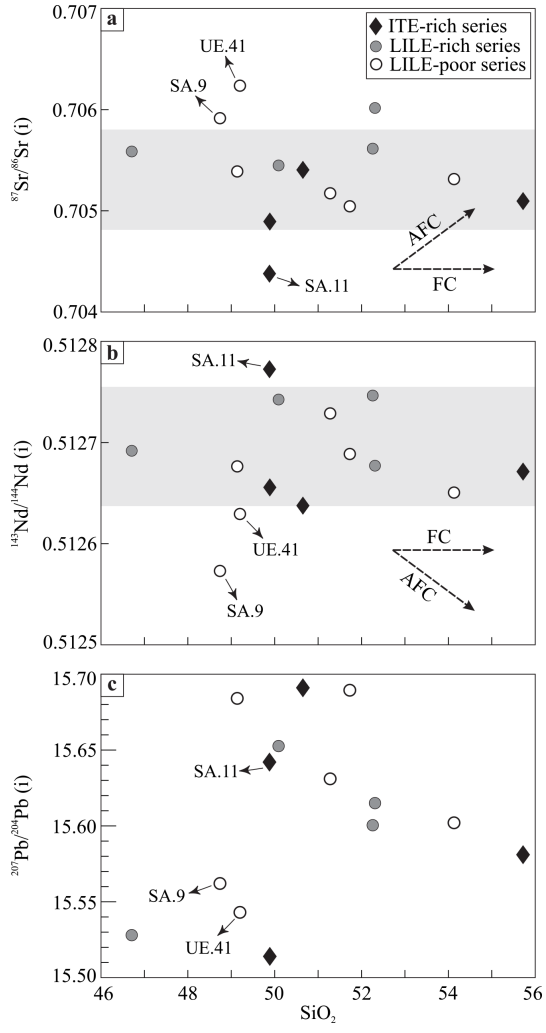


**Figure 5.** Plots of **(a)** $^{143}Nd/^{144}Nd_{(i)}$, **(b)** $^{87}Sr/^{86}Sr_{(i)}$, and **(c)** $^{207}Pb/^{204}Pb_{(i)}$ vs. $SiO_2$ (used as a fractionation index) for the LILE-rich, LILE-poor, and ITE-rich series of mafic volcanic rocks from the central UDMA – details in the text. Gray areas/bands mark restricted Sr–Nd isotopic variation for most of the mafic volcanic rocks. One sample from the ITE-rich series plots toward less-radiogenic Sr–Nd isotopic ratios (see Sect. 6.5 and Fig. 4a for details). Two samples from the LILE-poor series plot toward more-radiogenic Sr–Nd isotopic ratios; this is due to the higher slab components (i.e., slab + sediment) involvement (see Sect. 6.6 and Fig. 4a).

LILE-rich series melts, whereas melting of the mantle metasomatized by the partial melt of the same but dehydrated slab segment (i.e., fluid-poor slab melt) is likely to have led to the LILE-poor series melts. This is consistent with the more Mg-rich composition of the latter (Fig. 2). This occurs because the mantle with lower lithophiles and volatiles has a higher solidus and is more magnesian in composition (Pickering-Witter and Johnston, 2000).

The contribution of more fluids in the evolution of the LILE-rich series is implied by trace-element ratio plots (Fig. 7). The phase–equilibria relation is also in line with this model (i.e., fluid-rich slab melt versus fluid-poor slab melt involvement in the petrogenesis of the LILE-rich and LILE-poor series respectively). Higher mobile incompatible-element abundances of the primitive melt in the LILE-rich series are consistent with the geochemical evolution of the LILE-rich series; that is, the hydrous nature of the LILE-rich primitive melt depressed plagioclase fractionation and thereby prompted an early Al increase in the 48 wt %–52 wt % silica range in the series. Two different scenarios are raised here that may account for the petrogenesis of these two major rock series.

### 6.4.1 The slab rollback scenario

Considering the emphasis that has recently been made in regard to the application of the slab rollback model in the petrogenesis of the Cenozoic magmatic arc of Iran (Agard et al., 2005; Verdel et al., 2011; Yeganehfar et al., 2013; Babazadeh et al., 2017; Moradi et al., 2021), one may prompt a two-stage mantle metasomatism model as being responsible for the petrogenesis of the two series of volcanic rocks from the study area as follows. Slab dehydration at a given depth produced the "lithophile enriched" source mantle that generated the LILE-rich series melts. Gradual deepening (or rollback) of the dehydrated, lithophile-depleted slab was associated with an increasing temperature that prompted partial melting of the slab. This slab melt was depleted in lithophiles but enriched the overlying mantle in "immobile, highly incompatible elements". Due to the involvement of slab partial melts, the LILE-poor series melts are enriched in the immobile trace elements Nb to P (i.e., on the normalized trace-element patterns; Fig. 3), as compared to the LILE-rich series. This scenario, however, does not stand up to close scrutiny. Reviews of the age-dated mafic volcanic rocks from the study area (Ghorbani et al., 2014; see Fig. 3) and nearby areas (Ghorbani and Bezenjani, 2011; Yeganehfar et al., 2013; see Figs. S4 and S5 in the Supplement) do not indicate that the LILE-poor series postdate the LILE-rich series.

### 6.4.2 The simultaneous fluid-rich slab melt and fluid-poor slab melt mantle metasomatism scenario

It is suggested here that fluid-rich and fluid-poor slab-melt metasomatism, leading to the development of the LILE-rich and the LILE-poor series, took place concurrently, or within a short time span, along the entire magmatic arc. Young hot slabs are capable of yielding partial melts at sub-arc depths that correspond to the volcanic front (Hermann and Spandler, 2008; Manea et al., 2014; Zheng, 2019). Hot slab subduction of a then-narrow, almost vanished Neotethyan oceanic plate has likely been responsible for petrogenesis of slab melts that metasomatized source mantles of the three rock series: the LILE-rich, LILE-poor, and ITE-rich series. Disappearance

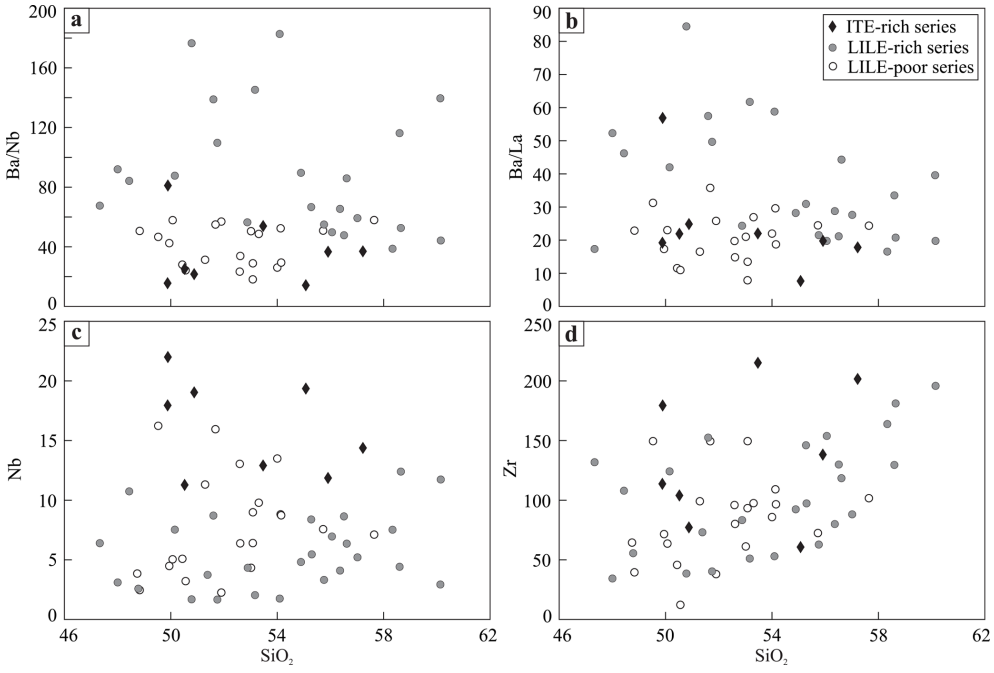


**Figure 6.** Plots of $SiO_2$ versus **(a)** Ba/Nb, **(b)** Ba/La, **(c)** Nb, and **(d)** Zr used for discrimination of LILE-rich, LILE-poor, and ITE-rich series (see text for details).

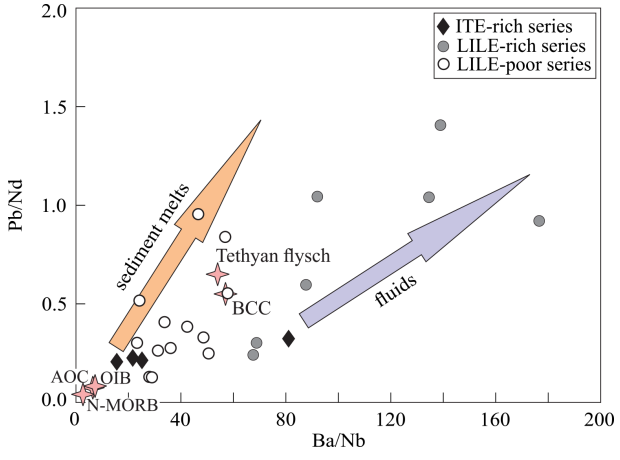


**Figure 7.** Ba/Nb versus Pb/Nd plot for the mafic volcanic rocks ($SiO_2 < 52$ wt %) from the study area. Higher mobile/immobile trace-element ratios in the LILE-rich series indicate the involvement of higher fluid in the petrogenesis of this series (e.g., Duggen et al., 2007; Straub et al., 2015). For references of the components involved (OIB, N-MORB, AOC, Tethyan flysch), see the caption for Fig. 4.

and termination of the Neotethyan oceanic slab are estimated to have predated the early Cenozoic (Agard et al., 2005; Horton et al., 2008; Dargahi et al., 2010). The rocks of the LILE-rich and LILE-poor series are mainly spatially constrained to occur toward the northern and central parts of the study area, namely the Kahak and Ardestan areas respectively. This implies a more hydrated, more altered nature of the northern segment of the slab subducting in the Kahak area, whereas the segment of the slab subducting in the Ardestsan area is deemed to have been of a higher $T$ (i.e., they may have been thicker and thinner slabs respectively).

### 6.5 The incompatible trace-element-rich (ITE-rich) series (including OIB-like samples)

Samples from the ITE-rich series are enriched in a wide range of incompatible trace elements that include lithophiles, La, Ce, Pb, Sr, and P, so they are called the incompatible trace-element-rich series, or ITE-rich series (Fig. 3). These include the most Nb–Ta enriched samples from the study area that approach the OIB pattern and, therefore, may be called OIB-like samples. However, they are not genuine OIBs because (1) their trace-element patterns are rather differentiated (i.e., as compared to the smooth trace patterns of the OIBs; Fig. 3), (2) their trace-element abundances are not as high as OIBs, and (3) their Sr–Nd–Pb isotopic signatures partly overlap those of the LILE-rich and LILE-poor series (Fig. 4). However, Sr and Nd isotopic ratios for the ITE-rich series extend toward lower and higher values respectively (i.e., as compared to the LILE-rich and LILE-poor series).

Samples from the ITE-rich series are more like high-Nb basalts (HNBs; Defant et al., 1992). The occurrence of HNBs in the subduction framework is attributed to either a mantle plume (i.e., an asthenospheric or OIB-type mantle) or a metasomatized mantle wedge (Reagan and Gill, 1989; Castillo et al., 2007). The HNBs are also known to be the mixing

products of an enriched (e.g., OIB-type) and a depleted (e.g., arc-type) source mantle (Hastie et al., 2011; Ahmadvand et al., 2021; Akbari et al., 2022). The ITE-rich series is suggested to have been generated by a slab-window or slab-tearing process at moderate pressures, whereby the underlying asthenospheric mantle penetrated into and facilitated slab partial melting that interacted with, and metasomatized, the mantle to produce the ITE-rich series (Benoit et al., 2002). The OIB trace-element pattern for sample SA.11 from the ITE-rich series (Fig. 3) supports asthenospheric mantle involvement. On the Sr–Nd isotopic plot, this sample deviates further toward and plots within the mantle array compared to the other samples from the ITE-rich series (see caption in Fig. 5).

### 6.6 Slab/crustal contributions to the arc magmatism

As differentiation by fractional crystallization (FC; see above) proceeds in a magmatic series, the more evolved melts show higher abundances of incompatible trace elements (e.g., Zheng, 2019). This is because the fractionated mineral assemblage has low Kd for the incompatible trace elements. However, in some batches of differentiated samples, the spate of increasing abundances of a few incompatible trace elements such as Th, K, La, and Ce exceeds that of other incompatible trace elements. These elements are believed to indicate crustal contamination or assimilation – processes which are usually associated with assimilation–fractional crystallization (AFC). Arc mafic volcanic rocks, due to the rather high ascent rate of mafic melts, are less likely to have undergone significant continental crustal contamination. Hence, their crustal signatures have probably been derived from the slab (i.e., slab plus sediment) fluids and melts that metasomatized the overlying mantle wedge (e.g., Benoit et al., 2002).

The origin and evolution of mafic volcanic rocks are best represented by the Sr–Nd–Pb isotopic ratios. The three series of volcanic rocks from the UDMA (i.e., the LILE-poor, LILE-rich, and ITE-rich series) plot on the same area of the Sr–Nd isotopic plot as other orogenic volcanic rocks and on the same area as other mafic volcanic rocks from the UDMA (Fig. 4). However, subtle but significant differences are observed in the distribution of the three series on this plot. Toward lower Sr isotopic ratios, data points of the three series converge to share a narrow space in the mantle array close to the BSE. The Sr–Nd isotopic variation trends expand toward higher Sr and lower Nd isotopic ratios (Fig. 4a). Increasing Sr isotopic ratios occur at constant Nd isotopic ratios in the LILE-rich series, whereas in the LILE-poor and ITE-rich series, the Sr isotopic ratios increase as Nd isotopic ratios decrease (Fig. 4a).

On Pb–Pb isotopic variation diagrams (Fig. 4b and c), the least-radiogenic members of the three series of mafic volcanic rocks – the LILE-poor, LILE-rich, and ITE-rich series – plot on the DMM–OIB mantle array (i.e., in the moderately depleted mantle area of the NHRL). The more differentiated volcanic rocks demonstrate sharp enrichment trends toward radiogenic Pb end-members on the Pb–Pb isotopic plots. Interestingly, the three series of volcanic rocks share one variation trend on these plots; this means that the fluid-rich slab melt and fluid-poor slab melt (i.e., the melts responsible for development of the LILE-rich and LILE-poor series respectively) maintain the same Pb isotopic ratios. This implies the finding that unlike different LILE / MREE ratios in the slab components involved in the petrogenesis of the LILE-rich and LILE-poor series, these slab-derived components have the same U content and U/Th ratio.

It was noted above that the geochemistry does not support continental crustal contamination (see Fig. 5). The isotopes are not fully discriminant to support the trace-element classification of mafic volcanic rocks into the three series presented here. However, the isotopes may be utilized to evaluate/estimate the geochemical reservoirs involved in their petrogenesis. Assuming a negligible continental crustal contamination in the evolution of the UDMA mafic volcanic rocks and utilizing the Sr–Nd isotopic data, ternary mixing modeling was carried out and showed that the UDMA mafic volcanic rocks can best be explained by mantle wedge and slab (i.e., including slab melt and sediment melt) participation.

The mantle wedge, slab, and slab sediment are represented by the average concentration of Kamchatka arc volcanic rocks (Kepezhinskas et al., 1997), altered oceanic crust (AOC; Hauff et al., 2003), and the Tethyan flysch sandstone sample 06FL03 from Serbia (Prelević et al., 2008) respectively. The ternary mixing model applied to the data of the UDMA mafic rocks found, in the LILE-rich and LILE-poor series, mantle wedge : slab contributions were 45 : 55 and 55 : 45 respectively. Numbers marked on the red and blue mixing curves in the inset of Fig. 4a indicate slab involvement in the petrogenesis of the LILE-rich and LILE-poor series was 50 %–60 % and 40 %–50 % respectively. For simplicity, these ranges are presented as mean values of 55 % and 45 %. The green curve is not recommended as a mixing model for the development of the ITE-rich series. As mentioned earlier, the ITE-rich series has likely been generated in a process similar to the one that led to the high-Nb basalts (Sect. 6.5).

The interception of the red and blue mixing curves with the slab melt–slab sediment array marks the proportion of slab melt : sediment melt involved in the petrogenesis of the LILE-rich and LILE-poor series (i.e., 50 : 50 and 20 : 80) respectively. Combining these two data sets, mantle wedge : slab melt : sediment melt proportions of 45 : 27.5 : 27.5 and 55 : 09 : 36 are obtained for the LILE-rich and LILE-poor series respectively. Mafic volcanic rocks from the western Nain area of the central UDMA (Yeganehfar et al., 2013) with trace-element patterns that mimic the LILE-rich, LILE-poor, and ITE-rich series patterns (Fig. S5) show Sr–Nd–Pb isotopic characteristics that are similar to the respec-

tive series from the study area, further supporting the petrogenetic model presented here (Fig. S6 in the Supplement).

Although the least evolved mafic volcanic rocks from the UDMA are presented in this study, volcanic rocks from the Nodoushan (i.e., southeastern segment of the study area) are still highly differentiated (see Sect. 6.3 and Fig. S3b). The Nodoushan rocks also show significant crustal contamination signatures, such as elevated lithophiles, Th, Pb, La–Ce, and Sr isotopic ratios. Some of the volcanic rocks show the highest Sr isotopic ratios from the study area. Hence, they are not included in the isotopic modeling. One of the Nodoushan rocks shows the highest Nd isotopic ratios, indicating the likely involvement of a more depleted mantle source.

## 7 Conclusions (spatio-temporal evolution of the UDMA volcanic-rock series and its implications)

The trace-element and Sr–Nd–Pb isotopic geochemistry of the mafic volcanic rocks from the Urumieh–Dokhtar magmatic arc (UDMA) of Iran indicate a metasomatized mantle origin and suggest a ternary classification into LILE-rich, LILE-poor and ITE-rich series. This is interpreted to represent the nature of the metasomatizing agents involved (i.e., the fluid-rich slab melt, the fluid-poor slab melt, and more-fertile segments of the mantle) in the development of the three series. A scrutiny of the ages of the volcanic rocks of the three series' compositional affinities (i.e., the LILE-rich, LILE-poor, and ITE-rich series) indicates Eocene to Early Miocene ages for all three. The Neotethyan plate predating the Eocene was likely to have been narrow, about to terminate, and hot enough to furnish the partial melts that metasomatized the source mantle. The physiochemical conditions that governed slab subduction in the northern and central parts of the study area, Kahak and Ardestan respectively, were slightly different but still have significant implications. The slab subducting in the Kahak area was more hydrous, producing fluid-rich slab melts, whereas the slab subducting in the Ardestan area was thinner and of higher $T$, producing fluid-poor slab melts. Similarities shared between Sr–Nd–Pb isotopic compositions and other contemporary arc-type UDMA mafic volcanic rocks suggest a source modified by recycled slab (slab + sediment). Isotopic modeling indicates that the mafic volcanic UDMA rocks from the LILE-rich and LILE-poor series were derived from juvenile metasomatized mantles with mantle : slab contributions of 45 : 55 and 55 : 45 respectively and where the slab melt : sediment melt involvement was 50 : 50 and 20 : 80. The ITE-rich series bear signatures of source-mantle metasomatism by slab melts that were prompted by, and interacted with, asthenospheric melts in a slab window.

*Data availability.* Data are available in the EarthChem Library and can be accessed via a DOI link at https://doi.org/10.60520/IEDA/113464 (Ghorbani et al., 2025).

*Supplement.* The Supplement contains Tables S1–S5 and Figs. S1–S6. The supplement related to this article is available online at https://doi.org/10.5194/se-16-663-2025-supplement.

*Author contributions.* MRG: conceptualization, data curation, formal analysis, funding acquisition, investigation, methodology, project administration, resources, supervision, validation, visualization, and writing (original draft preparation as well as paper review and editing). MA: conceptualization, data curation, formal analysis, investigation, methodology, project administration, resources, software, supervision, validation, visualization, writing (original draft preparation as well as paper review and editing). ITG: conceptualization, data curation, formal analysis, funding acquisition, resources, software, validation, visualization, and writing (review and editing). MB: conceptualization, data curation, formal analysis, funding acquisition, investigation, methodology, resources, software, validation, visualization, and writing (review and editing). FS: conceptualization, data curation, formal analysis, validation, visualization, and writing (review and editing).

*Competing interests.* The contact author has declared that none of the authors has any competing interests.

*Disclaimer.* Publisher's note: Copernicus Publications remains neutral with regard to jurisdictional claims made in the text, published maps, institutional affiliations, or any other geographical representation in this paper. While Copernicus Publications makes every effort to include appropriate place names, the final responsibility lies with the authors.

*Acknowledgements.* This work is a part of the sabbatical leave that the first author spent at the University of New South Wales (UNSW, Sydney, Australia) in early 2023 as well as a part of his long-term research interest in arc magmatism at Tarbiat Modares University (TMU, Iran). Isotopic analytical facilities provided by the GET-OMP (Toulouse, France) are sincerely appreciated. Valuable comments by Pier Paolo Giacomoni and Delphine Bosch are highly appreciated; these comments helped significantly improve the paper. The insightful handling of the paper by Massimo Coltorti is sincerely appreciated. We would also like to thank Helen Wang and Irene Wainwright from the X-ray Fluorescence Laboratory (UNSW, Sydney, Australia) for the XRF analyses and Alan Greig from the School of Geography, Earth and Atmospheric Sciences (University of Melbourne, Victoria, Australia) for the ICP–MS analyses.

*Review statement.* This paper was edited by Massimo Coltorti and reviewed by Delphine Bosch.

## References


Agard, P., Omrani, J., Jolivet, L., and Mouthereau, F.: Convergence history across Zagros (Iran): Constraints from collisional and earlier deformation, Int. J. Earth Sci., 94, 401–419, https://doi.org/10.1007/s00531-005-0481-4, 2005.

Ahmadian, J., Sarjoughian, F., Lentz, D., Esna-Ashari, A., Murata, M., and Ozawa, H.: Eocene K-rich adakitic rocks in the Central Iran: Implications for evaluating its Cu-Au-Mo metallogenic potential, Ore Geol. Rev., 72, 323–342, https://doi.org/10.1016/j.oregeorev.2015.07.017, 2016.

Ahmadvand, A., Ghorbani, M. R., Mokhtari, M. A. A., Chen, Y., Amidon, W., Santos, J. F., and Paydari, M.: Lithospheric mantle, asthenosphere, slab and crustal contribution to petrogenesis of Eocene to Miocene volcanic rocks from the west Alborz magmatic assemblage, SE Ahar, Iran, Geol. Mag., 158, 375–406, https://doi.org/10.1017/S0016756820000527, 2021.

Akbari, M., Ghorbani, M. R., Cousens, B. L., and Graham, I. T.: Quaternary post-collisional high Nb-like basalts from Bijar-Qorveh, NW Iran: a metasomatized lithospheric mantle source, Lithos, 426–427, 106781, https://doi.org/10.1016/j.lithos.2022.106781, 2022.

Akbari, M., Ghorbani, M. R., Cousens, B. L., and Graham, I. T.: A robust discrimination scheme for ocean island basalts based on Ce/Rb, Tb/La, and Ba/Nb ratios, Chem. Geol., 628, 121486, https://doi.org/10.1016/j.chemgeo.2023.121486, 2023.

Alaie-Mahabadi, S. and Foudazi, M.: Geological map of the Nain quadrangle, Geological Survey of Iran, scale 1 : 100 000, 1 sheet, 2004.

Alavi, M.: Tectonics of the Zagros orogenic belt of Iran: New data and interpretations, Tectonophysics, 229, 211–238, https://doi.org/10.1016/0040-1951(94)90030-2, 1994.

Amidi, S. M., Nabavi, M. H., and Molla Ali, A.: Geological map of the Sarve-Bala quadrangle, Geological Survey of Iran, scale 1 : 100 000, 1 sheet, 1989.

Amini, B. and Amini Chehragh, M. R.: Geological map of the Kajan quadrangle, Geological Survey of Iran, scale 1 : 100 000, 1 sheet, 2003.

Atanasova, P., Marks, M. A. W., Frenzel, M., Gutzmer, J., Krause, J., and Markl, G.: Fractionation of geochemical twins (Zr/Hf, Nb/Ta and Y/Ho) and HREE-enrichment during magmatic and metamorphic processes in peralkaline nepheline syenites from Norra Kärr (Sweden), Lithos, 372–373, 105667, https://doi.org/10.1016/j.lithos.2020.105667, 2020.

Babazadeh, S., Ghorbani, M. R., Bröcker, M., D'Antonio, M., Cottle, J., Gebbing, T., Mazzeo, F. C., and Ahmadi, P.: Late Oligocene-Miocene mantle upwelling and interaction inferred from mantle signatures in gabbroic to granitic rocks from the Urumieh–Dokhtar arc, south Ardestan, Iran, Int. Geol. Rev., 59, 1590–1608, https://doi.org/10.1080/00206814.2017.1286613, 2017.

Bahroudi, A. and Fonoudi, M.: Geological map of the Shahrab quadrangle, Geological Survey of Iran, scale 1 : 100 000, 1 sheet, 1997.

Benoit, M., Aguillón-Robles, A., Calmus, T., Maury, R. C., Bellon, H., Cotton, J., Bourgois, J., and Michaud, F.: Geochemical diversity of Late Miocene volcanism in southern Baja California, Mexico: Implication of mantle and crustal sources during the opening of an asthenospheric window, J. Geol., 110, 627–648, https://doi.org/10.1086/342735, 2002.

Berberian, F. and Berberian, M.: Tectono-plutonic episodes in Iran, in: Zagros, Hindu Kush, Himalaya geodynamic evolution, edited by: Delany, F. M. and Gupta, H. K., Geodynamics Series, vol. 3, Am. Geophys. Union, 5–32, 1981.

Berberian, M. and King, G. C. P.: Towards a paleogeography and tectonic evolution of Iran, Can. J. Earth Sci., 18, 210–265, https://doi.org/10.1139/e81-019, 1981.

Bouilhol, P., Jagoutz, O., Hanchar, J. M., and Dudas, F. O.: Dating the India-Eurasia collision through arc magmatic records, Earth Planet. Sc. Lett., 366, 163–175, https://doi.org/10.1016/j.epsl.2013.01.023, 2013.

Castillo, P. R., Rigby, S. J., and Solidum, R. U.: Origin of high field strength element enrichment in volcanic arcs: Geochemical evidence from the Sulu Arc, southern Philippines, Lithos, 97, 271–288, https://doi.org/10.1016/j.lithos.2006.12.012, 2007.

Chauvel, C., Lewin, E., Carpentier, M., Arndt, N. T., and Marini, J. C.: Role of recycled oceanic basalt and sediment in generating the Hf-Nd mantle array, Nat. Geosci., 1, 64–67, https://doi.org/10.1038/ngeo.2007.51, 2008.

Chiu, H. Y., Chung, S. L., Zarrinkoub, M. H., Mohammadi, S. S., Khatib, M. M., and Iizuka, Y.: Zircon U-Pb age constraints from Iran on the magmatic evolution related to Neotethyan subduction and Zagros orogeny, Lithos, 162–163, 70–87, https://doi.org/10.1016/j.lithos.2013.01.006, 2013.

Cross, T. A. and Pilger, R. H.: Controls of subduction geometry, location of magmatic arcs, and tectonics of arc and back-arc regions, Geol. Soc. Am. Bull., 93, 545–562, https://doi.org/10.1130/0016-7606(1982)93<545:COSGLO>2.0.CO;2, 1982.

Dargahi, S., Arvin, M., Pan, Y., and Babae, A.: Petrogenesis of post-collisional A-type granitoids from the Urumieh–Dokhtar magmatic assemblage, South western Kerman, Iran: Constraints on the Arabian–Eurasian continental collision, Lithos, 115, 190–204, https://doi.org/10.1016/j.lithos.2009.12.002, 2010.

Defant, M. J., Jackson, T. E., Drummond, M. S., De Boer, J. Z., Bellon, H., Feigenson, M. D., Maury, R. C., and Stewart, R. H.: The geochemistry of young volcanism throughout western Panama and southeastern Costa Rica: An overview, J. Geol. Soc. London, 149, 569–579, https://doi.org/10.1144/gsjgs.149.4.0569, 1992.

Di Giuseppe, P., Agostini, S., Di Vincenzo, G., Manetti, P., Savaşçın, M. T., and Conticelli, S.: From subduction to strike sliprelated volcanism: insights from Sr, Nd, and Pb isotopes and geochronology of lavas from Sivas-Malatya region, Central Eastern Anatolia, Int. J. Earth Sci., 110, 849–874, https://doi.org/10.1007/s00531-021-01995-0, 2021.

Dong, K., Chen, S., Graham, I., Zhao, J., Fu, P., Xu, Y., Tian, G., Qin, W., and Chen, J.: Geochemical behavior during mineralization and alteration events in the Baiyinchang volcanic-hosted massive sulfide deposits, Gansu Province, China, Ore Geol. Rev., 91, 559–572, https://doi.org/10.1016/j.oregeorev.2017.09.002, 2017.

Duggen, S., Portnyagin, M., Baker, J., Ulfbeck, D., Hoernle, K., Garbe-Schönberg, D., and Grassineau, N.: Drastic shift in lava geochemistry in the volcanic-front to rear-arc region of the Southern Kamchatkan subduction zone: Evidence for the transition from slab surface dehydration to sediment melting, Geochim. Cosmochim. Ac., 71, 452–480, https://doi.org/10.1016/j.gca.2006.09.018, 2007.

Emami, M. H., Sadeghi, M. M. M., and Omrani, S. J.: Magmatic map of Iran, Geological Survey of Iran, Tehran, 1993.

Ewart, A., Collerson, K. D., Regelous, M., Wendt, J. I., and Niu, Y.: Geochemical evolution within the Tonga-Kermadec-Lau arc-back-arc systems: the role of varying mantle wedge composition in space and time, J. Petrol., 39, 331–368, https://doi.org/10.1093/petroj/39.3.331, 1998.

Farner, M. J. and Lee, C. A.: Effects of crustal thickness on magmatic differentiation in subduction zone volcanism: A global study, Earth Planet. Sc. Lett., 470, 96–107, https://doi.org/10.1016/j.epsl.2017.04.025, 2017.

Ghalamghash, J., Babakhani, A. R., Bahroudi, A., and Fonoudi, M.: Geological map of the Kahak quadrangle, Geological Survey of Iran, scale 1 : 100 000, 1 sheet, 1988.

Ghalamghash, J., Mohammadiha, K., and Ghahraie Pour, M.: Geological map of the Kafeh-Taghestan quadrangle, Geological Survey of Iran, scale 1 : 100 000, 1 sheet, 2005.

Ghorbani, M. R.: Lead enrichment in Neotethyan volcanic rocks from Iran: The implications of a descending slab, Geochem. J., 40, 557–568, https://doi.org/10.2343/geochemj.40.557, 2006.

Ghorbani, M. R. and Bezenjani, R. N.: Slab partial melts from the metasomatizing agent to adakite, Tafresh Eocene volcanic rocks, Iran, Isl. Arc, 20, 188–202, https://doi.org/10.1111/j.1440-1738.2010.00757.x, 2011.

Ghorbani, M. R. and Middlemost, E. A. K.: Geochemistry of pyroxene inclusions from the Warrumbungle Volcano, New South Wales, Australia, Am. Mineral., 85, 1349–1367, https://doi.org/10.2138/am-2000-1003, 2000.

Ghorbani, M. R., Graham, I. T., and Ghaderi, M.: Oligocene-Miocene geodynamic evolution of the central part of Urumieh-Dokhtar arc of Iran, Int. Geol. Rev., 56, 1039–1050, https://doi.org/10.1080/00206814.2014.919615, 2014.

Ghorbani, M. R., Akbari, M., Graham, I. T., Benoit, M., Sepidbar, F., and Zwingmann, H.: Trace and major elements and Sr-Nd-Pb isotopic data from the Urumieh-Dokhtar magmatic arc of Iran, Version 1.0, Interdisciplinary Earth Data Alliance (IEDA) [data set], https://doi.org/10.60520/IEDA/113464, 2025.

Gill, J. B.: Orogenic Andesites and Plate Tectonics, Springer-Verlag, New York, https://doi.org/10.1007/978-3-642-68012-0, 1981.

Hart, S. R.: A large-scale isotope anomaly in the Southern Hemisphere mantle, Nature, 309, 753–757, https://doi.org/10.1038/309753a0, 1984.

Hastie, A. R., Mitchell, S. F., Kerr, A. C., Minifie, M. J., and Millar, I. L.: Geochemistry of rare high-Nb basalt lavas: are they derived from a mantle wedge metasomatised by slab melts?, Geochim. Cosmochim. Ac., 75, 5049.72, https://doi.org/10.1016/j.gca.2011.06.018, 2011.

Hauff, F., Hoernle, K., and Schmidt, A.: Sr–Nd–Pb composition of Mesozoic Pacific oceanic crust (Site 1149 and 801, ODP Leg 185): Implications for alteration of ocean crust and the input into the Izu–Bonin–Mariana subduction system, Geochem. Geophy. Geosy., 4, 1–30, https://doi.org/10.1029/2002GC000421, 2003.

Hawkesworth, C., Turner, S., Peate, D., McDermott, F., and Calsteren, P. V.: Elemental U and Th variations in island arc rocks: implications for U-series isotopes, Chem. Geol., 139, 207–221, https://doi.org/10.1016/S0009-2541(97)00036-3, 1997.

Hermann, J. and Spandler, C. J.: Sediment Melts at Sub-arc Depths: an Experimental Study, J. Petrol., 49, 717–740, https://doi.org/10.1093/petrology/egm073, 2008.

Hildreth, W. and Moorbath, S.: Crustal contributions to arc magmatism in the Andes of central Chile, Contrib. Mineral. Petr., 98, 455–489, https://doi.org/10.1007/BF00372365, 1988.

Horton, B. K., Hassanzadeh, J., Stockli, D. F., Axen, G. J., Gillis, R. J., Guest, B., Amini, A., Fakhari, M. D., Zamanzade, S. M., and Grove, M.: Detrital zircon provenance of Neoproterozoic to Cenozoic deposits in Iran: Implications for chronostratigraphy and collisional tectonics, Tectonophysics, 451, 97–122, https://doi.org/10.1016/j.tecto.2007.11.063, 2008.

Jicha, B. R. and Singer, B. S.: Volcanic history and magmatic evolution of Seguam Island, Aleutian Island arc, Alaska, Geol. Soc. Am. Bull., 118, 805–822, https://doi.org/10.1130/B25861.1, 2006.

Jolani Varzeghani, A.: Trace elements and isotope geochemistry of Nodoushan volcanic rocks, MSc Thesis, Tarbiat Modares University, Tehran, Iran, 2017.

Kelemen, P. B., Hanghøj, K., and Greene, A. R.: One view of the geochemistry of subduction-related magmatic arcs, with an emphasis on primitive andesite and lower crust, in: Treatise Geochem., 3. The Crust, edited by: Rudnick, R. L., Elsevier, Amsterdam, 593–659, https://doi.org/10.1016/B0-08-043751-6/03035-8, 2005.

Kepezhinskas, P. K., Defant, M. J., and Drummond, M. S.: Na metasomatism in the island-arc mantle by slab melt-peridotite interaction: evidence from mantle xenoliths in the North Kamchatka arc, J. Petrol., 36, 1505–1527, https://doi.org/10.1093/oxfordjournals.petrology.a037263, 1995.

Kepezhinskas, P., McDermott, F., Defant, M. J., Hochstaedter, A., Drummond, M. S., Hawkesworth, C. J., Kokoskov, A., Maury, R., and Bellon, H.: Trace element and Sr–Nd–Pb isotopic constraints on a three-component model of Kamchatka Arc petrogenesis, Geochim. Cosmochim. Ac., 61, 577–600, https://doi.org/10.1016/S0016-7037(96)00349-3, 1997.

Khalatbari Jafari, M. and Alaie-Mahabadi, S.: Geological map of the Natanz quadrangle, Geological Survey of Iran, scale 1 : 100 000, 1 sheet, 1995.

Khodami, M.: Pb isotope geochemistry of the late Miocene–Pliocene volcanic rocks from Todeshk, the central part of the Urumieh–Dokhtar magmatic arc, Iran: Evidence of an enriched mantle source, J. Earth Syst. Sci., 128, 167, https://doi.org/10.1007/s12040-019-1185-7, 2019.

Li, C. F., Li, X. H., Li, Q. L., Guo, J. H., and Li, X. H.: Directly determining $^{143}Nd/^{144}Nd$ isotope ratios using thermal ionization mass spectrometry for geological samples without separation of Sm–Nd, J. Anal. Atom. Spectrom., 26, 2012–2022, https://doi.org/10.1039/C0JA00081G, 2011.

Li, C. F., Li, X. H., Li Q. L. Guo, J. H., Li, X. H., and Yang, Y. H.: Rapid and precise determination of Sr and Nd isotopic ratios in geological samples from the same filament loading by thermal ionization mass spectrometry employing a single-step separation scheme, Anal. Chim. Acta, 727, 54–60, https://doi.org/10.1016/j.aca.2012.03.040, 2012.

Linnen, R. L. and Keppler, H.: Melt composition control of Zr/Hf fractionation in magmatic processes, Geochim. Cosmochim. Ac., 66, 3293–3301, https://doi.org/10.1016/S0016-7037(02)00924-9, 2002.

Manea, V. C., Leeman, W. P., Gerya, T., Manea, M., and Zhu, G.: Subduction of fracture zones controls mantle melting and geochemical signature above slabs, Nat. Commun., 5, 5095, https://doi.org/10.1038/ncomms6095, 2014.

Mayborn, K. R. and Lesher, C. E.: MagPath: An Excel-based Visual Basic program for forward modeling of mafic magma crystallization, Comput. Geosci., 3, 1900–1903, https://doi.org/10.1016/j.cageo.2011.02.017, 2011.

Mohajjel, M. and Fergusson, C. L.: Dextral transpression in Late Cretaceous continental collision, Sanandaj-Sirjan Zone, western Iran, J. Struct. Geol., 22, 1125–1139, https://doi.org/10.1016/S0191-8141(00)00023-7, 2000.

Moinevaziri, H.: Volcanisme Tertiaire et Quaternaire en Iran, Paris-Sud Orsay, Thèse d'État, 1985.

Moradi, S., Ghorbani, M. R., Jiang, S. Y., and Christiansen, E. H.: Mafic to intermediate composition intrusions from the Kahak area, central Urumieh-Dokhtar arc of Iran: transition from Eocene to Miocene intra-arc extensional magmatism, Miner. Petrol., 115, 445–466, https://doi.org/10.1007/s00710-021-00745-z, 2021.

Morishita, T., Arai, S., and Tamura, A.: Petrology of an apatite-rich layer in the Finero phlogopite–peridotite, Italian Western Alps; implications for evolution of a metasomatising agent, Lithos, 69, 37–49, https://doi.org/10.1016/S0024-4937(03)00046-X, 2003.

Norrish, K. and Hutton, J. T.: An accurate X-ray spectrographic method for the analysis of a wide range of geological samples, Geochim. Cosmochim. Ac., 33, 431–453, https://doi.org/10.1016/0016-7037(69)90126-4, 1969.

Omrani, J., Agard, P., Whitechurch, H., Benoit, M., Prouteau, G., and Jolivet, L.: Arc-magmatism and subduction history beneath the Zagros Mountains, Iran: A new report of adakites and geodynamic consequences, Lithos, 106, 380–398, https://doi.org/10.1016/j.lithos.2008.09.008, 2008.

O'Reilly, S. Y., Griffin, W. L., and Ryan, C. G.: Residence of trace elements in metasomatised spinel lherzolite xenoliths: A proton-microprobe study, Contrib. Mineral. Petr., 109, 98–113, https://doi.org/10.1007/BF00687203, 1991.

Pearce, J. A.: Trace element characteristics of lavas from destructive plate boundaries, in: Orogenic andesites and related rocks, edited by: Thorpe, R. S., John Wiley and Sons, Chichester, England, 528–548, ISBN 9780471280347, 1982.

Pearce, J. A., Bender, J. F., Delong, S. E., Kidd, W. S. F., Low, P. J., Guner, Y., Sargolu, F., Yilmaz, Y., Moorbath, S., and Mitchell, J. G.: Genesis of collision volcanism in eastern Anatolia, Turkey, J. Volcanol. Geoth. Res., 44, 189–229, https://doi.org/10.1016/0377-0273(90)90018-B, 1990.

Pickering-Witter, J. M. and Johnston, A. D.: The effects of variable bulk composition on the melting systematics of fertile peridotitic assemblages, Contrib. Mineral. Petr., 140, 190–211, https://doi.org/10.1007/s004100000183, 2000.

Pin, C. and Gannoun, A.: Integrated Extraction Chromatographic Separation of the Lithophile Elements Involved in Long-Lived Radiogenic Isotope Systems (Rb–Sr, U–Th–Pb, Sm–Nd, La–Ce, and Lu–Hf) Useful in Geochemical and Environmental Sciences, Anal. Chem., 89, 2411–2417, https://doi.org/10.1021/acs.analchem.6b04289, 2017.

Plank, T. and Langmuir, C. H.: An evaluation of the global variations in the major element chemistry of arc basalts, Earth Planet. Sc. Lett., 90, 349–370, https://doi.org/10.1016/0012-821X(88)90135-5, 1988.

Powell, R.: Inversion of the assimilation and fractional crystallization (AFC) equations; characterization of contaminants from isotope and trace element relationships in volcanic suites, J. Geol. Soc., 141, 447–452, https://doi.org/10.1144/gsjgs.141.3.0447, 1984.

Prelević, D., Foley, S. F., Romer, R., and Sonticelli, S.: Mediterranean Tertiary lamproites derived from multiple source components in postcollisional geodynamics, Geochim. Cosmochim. Ac., 72, 2125–2156, https://doi.org/10.1016/j.gca.2008.01.029, 2008.

Rabiee, A., Rossetti, F., Asahara, Y., Azizi, H., Lucci, F., Lustrino, M., and Nozaem, R.: Long-lived, Eocene-Miocene stationary magmatism in NW Iran along a transform plate boundary, Gondwana Res., 85, 237–262, https://doi.org/10.1016/j.gr.2020.03.014, 2020.

Radfar, J. and Alaie-Mahabadi, S.: Geological map of the Kashan quadrangle, Geological Survey of Iran, scale 1 : 100 000, 1 sheet, 1993.

Radfar, J. and Amini Chehragh, M. R.: Geological map of the Ardestan quadrangle, Geological Survey of Iran, scale 1 : 100 000, 1 sheet, 1999.

Radfar, J., Kohansal, R., and Zolfaghari, S.: Geological map of the Kuhpayeh quadrangle, Geological Survey of Iran, scale 1 : 100 000, 1 sheet, 2002.

Reagan, M. K. and Gill, J. B.: Coexisting calcalkaline and high-niobium basalts from Turrialba volcano, Costa Rica: implications for residual titanites in arc magma sources, J. Geophys. Res., 94, 4619–4633, https://doi.org/10.1029/JB094iB04p04619, 1989.

Schiano, P., Clocchiatti, R., Shimizu, N., Maury, R. C., Jochum, K. P., and Hofmann, A. W.: Hydrous, silica-rich melts in the sub-arc mantle and their relationship with erupted arc lavas, Nature, 377, 595–600, https://doi.org/10.1038/377595a0, 1995.

Sepidbar, F., Shafaii Moghadam, H., Zhang, L., Li, J. W., Ma, J., Stern, R. J., and Lin, C.: Across–arc geochemical variations in the Paleogene magmatic belt of Iran, Lithos, 344–345, 280–396, https://doi.org/10.1016/j.lithos.2019.06.022, 2019.

Sepidbar, F., Karsli, O., Palin, R. M., and Casetta, F.: Cenozoic temporal variation of crustal thickness in the Urumieh-Dokhtar and Alborz magmatic belts, Iran, Lithos, 400–401, 106401, https://doi.org/10.1016/j.lithos.2021.106401, 2021.

Shafaii Moghadam, H., Ghorbani, G., Zaki Khedr, M., Fazlnia, N., Chiaradia, M., Eyuboglu, Y., Santosh, M., Francisco, C. G., Martinez, M, L., Gourgaud, A., and Arai, S.: Late Miocene K-rich volcanism in the Eslamieh Peninsula (Saray), NW Iran: Implications for geodynamic evolution of the Turkish–Iranian High Plateau, Gondwana Res., 26, 1028–1050, https://doi.org/10.1016/j.gr.2013.09.015, 2014.

Shahabpour, J.: Island-arc affinity of the central Iranian volcanic belt, J. Asian Earth Sci., 30, 652–665, https://doi.org/10.1016/j.jseaes.2007.02.004, 2007.

Spikings, R., Cochrane, R., Villagomez, D., Van der Lelij, R., Vallejo, C., Winkler, W., and Beate, B.: The Geological History of Northwestern South America: from Pangaea to the Early Collision of the Caribbean Large Igneous Province (290–75 Ma), Gondwana Res., 27, 95–139, https://doi.org/10.1016/j.gr.2014.06.004, 2015.

Stracke, A., Bizimis, M., and Salters, V. J. M.: Recycling oceanic crust: quantitative constraints, Geochem. Geophy. Geosy., 4, 8003, https://doi.org/10.1029/2001GC000223, 2003.

Stracke, A., Hofmann, A. W., and Hart, S. R.: FOZO, HIMU, and the rest of the mantle zoo, Geochem. Geophy. Geosy., 6, Q05007, https://doi.org/10.1029/2004GC000824, 2005.

Straub, S. M., Gómez-Tuena, A., Bindeman, I. N., Bolge, L. L., Brandle, P. A., Espinasa-Perena, R., Solari, L., Stuart, F. M., Vannucchi, P., and Zellmer, G. F.: Crustal recycling by subduction erosion in the central Mexican Volcanic Belt, Geochim. Cosmochim. Ac., 166, 29–52, https://doi.org/10.1016/j.gca.2015.06.001, 2015.

Streck, M. J., Leeman, W. P., and Chesley, J.: High-magnesian andesite from Mount Shasta: a product of magma mixing and contamination, not a primitive mantle melt, Geology, 35, 351–354, https://doi.org/10.1130/G23286A.1, 2007.

Sun, S. S. and McDonough, W. F.: Chemical and isotopic systematics of oceanic basalts: Implications for mantle composition and processes, J. Geol. Soc., London, Special Publications, 42, 313–345, https://doi.org/10.1144/gsl.sp.1989.042.01.19, 1989.

Szabó, C., Falus, G., Zajacz, Z., Kovács, I., and Bail, E.: Composition and evolution of lithosphere beneath the Carpathian-Pannonian Region: a review, Tectonophysics, 393, 119–137, https://doi.org/10.1016/j.tecto.2004.07.031, 2004.

van Hinsbergen, D. J. J., Torsvik, T. H., Schmid, S. M., Maţenco, L. C., Maffione, M., Vossers, R. L. M., Gürer, D., and Spakman, W.: Orogenic architecture of the Mediterranean region and kinematic reconstruction of its tectonic evolution since the Triassic, Gondwana Res., 81, 79–229, https://doi.org/10.1016/j.gr.2019.07.009, 2020.

Verdel, C., Wernicke, B. P., Hassanzadeh, J., and Guest, B.: A Paleogene extensional arc flare up in Iran, Tectonics, 30, 1–20, https://doi.org/10.1029/2010TC002809, 2011.

Wilson, B. M.: Igneous Petrogenesis: A Global Tectonic Approach, Chapman and Hall, London, https://doi.org/10.1007/978-1-4020-6788-4, 1989.

Xia, L. Q.: The geochemical criteria to distinguish continental basalts from arc related ones, Earth-Sci. Rev., 139, 195–212, https://doi.org/10.1016/j.earscirev.2014.09.006, 2014.

Yeganehfar, H., Ghorbani, M. R., Shinjo, R., and Ghaderi, M.: Magmatic and geodynamic evolution of Urumieh-Dokhtar basic volcanism, Central Iran: major, trace element, isotopic, and geochronologic implications, Int. Geol. Rev., 55, 767–786, https://doi.org/10.1080/00206814.2012.752554, 2013.

Zahedi, M. and Rahmati, M.: Geological map of the Tarq quadrangle, Geological Survey of Iran, scale 1 : 100 000, 1 sheet, 2002.

Zheng, Y. F.: Subduction zone geochemistry, Geosci. Front., 10, 1223–1254, https://doi.org/10.1016/j.gsf.2019.02.003, 2019.